Marine productivity, water column processes and seafloor anoxia in relation to Nile discharge during sapropels S1 and S3

Karin L. Zwiep [a, *, 1], Rick Hennekam [b, c, **, 1], Timme H. Donders [a, d],
Niels A.G.M. van Helmond [a, b], Gert J. de Lange [b], Francesca Sangiorgi [a]

[a] Marine Palynology and Paleoceanography, Department of Earth Sciences, Faculty of Geosciences, Utrecht University, Princetonlaan 8, 3584 CB, Utrecht, the Netherlands
[b] Geochemistry, Department of Earth Sciences, Faculty of Geosciences, Utrecht University, Princetonlaan 8, 3584 CB, Utrecht, the Netherlands
[c] NIOZ Royal Netherlands Institute for Sea Research, Department of Ocean Systems, and Utrecht University, P.O. Box 59, 1790 AB, Den Burg, Texel, the Netherlands
[d] Palaeoecology, Department of Physical Geography, Faculty of Geosciences, Utrecht University, Princetonlaan 8, 3584 CB, Utrecht, the Netherlands

ABSTRACT

Eastern Mediterranean sapropels S1 (~10.5—6.1 kyr BP) and S3 (~85.8—80.8 kyr BP) formed respectively under full interglacial and glacial inception conditions. Consequently, the environmental factors preconditioning and leading to sapropel formation (e.g., global sea level and monsoonal forcing) were different. These factors must have differently influenced processes such as marine productivity, water column processes, and related seafloor anoxia. Here we investigate these differences through an interdisciplinary approach using dinoflagellate cyst and pollen/spore assemblages and sedimentary (redox-sensitive) trace-metal concentrations from a core in the central Nile delta area. Comparing S1 to S3, we demonstrate that (1) Nile discharge appears to be stronger during S3 than S1, as shown by $\delta^{18}O_{residuals}$, higher ratio of pollen and spores, and the higher abundance of coastal dinocysts and freshwater palynomorphs, (2) Ba/Al, C_{org}, and dinocyst accumulation rates indicate that marine productivity was similar at least during the first phase of their deposition and started prior to the onset of both sapropels, (3) bottom water conditions were more reducing during S3, resulting in higher Mo/Al, S, and C_{org}/P_{tot} values, but preservation was high and similar for both sapropels, and (4) Sedimentary Mo-—U covariation indicates that the depth of water-column ventilation during deposition of S3 was shallower than during S1 (~1000 m versus ~1800m, respectively). We attribute the observed differences to slightly enhanced precessional-forced monsoon intensity and potentially lower global sea level, resulting not only in increased North-African run-off, but also in reduced ventilation during S3 compared to S1.

© 2018 Elsevier Ltd. All rights reserved.

1. Introduction

Organic-rich sediment layers, called sapropels, have been repeatedly deposited in the landlocked Eastern Mediterranean basin, at least since the Miocene (e.g. Rossignol-Strick, 1985; Hilgen, 1991; Rohling, 1994; Nijenhuis et al., 1996; Cramp and O'Sullivan, 1999). Two main mechanisms for sapropel formation have been proposed (see Rohling et al. (2015) for a review): 1) surface water buoyancy gain, due to enhanced precession-driven North African monsoon intensity fuelling North African river systems. This triggered water column stratification, reduced deep-water ventilation, and promoted organic-matter preservation (Rossignol-Strick, 1985; Rohling et al., 2002; Emeis et al., 2003); 2) Enhanced marine productivity due to nutrient injection into the photic zone (Krom et al., 2002), by river discharge, shoaling of the nutricline (Rohling and Gieskes, 1989; Grelaud et al., 2012), and/or upward advection of nutrients released from anoxic sediments (Slomp et al., 2002). This led to high export productivity, and increased the process of organic matter degradation and thus oxygen consumption at depth. Most likely, a combination of both ventilation and productivity

* Corresponding author.
** Corresponding author. NIOZ Royal Netherlands Institute for Sea Research, Department of Ocean Systems, and Utrecht University, P.O. Box 59, 1790 AB, Den Burg, Texel, the Netherlands.
E-mail addresses: k.l.zwiep@gmail.com (K.L. Zwiep), rickhennekam@gmail.com (R. Hennekam).
[1] Joint First Authors.

resulted in organic matter build-up in the sediments, but the relative contribution of each mechanism remains under discussion (Rohling et al., 2015).

Recent studies have suggested that a change in sea level and inflow of less saline Atlantic waters at Gibraltar during Heinrich stadials may have been important preconditioning factors for sapropel formation, particularly for the most recent Holocene sapropel S1 (~10.5–6.1 kyrs before present, BP) deposited during a rising sea-level trend (Grimm et al., 2015). The sea level pre-conditioning effect is considered less important for sapropels S3, S4, and S5 deposition, based on the timing of these sapropels relative to monsoon and sea-level variability (Grant et al., 2016). Studies of multiple sapropels from the same sedimentary record are needed to shed light into the role of Nile discharge and sea level in sapropel formation, while minimizing biases due different lo-cations (e.g., distance from the freshwater input source, deposition depth).

Sapropel S1 is the most studied sapropel, because it is the easiest to recover with coring devices and because radiocarbon can be used for accurate radiocarbon dating. However, advancements in dating of older Mediterranean sediments, i.e. through tuning of Eastern Mediterranean sediment records to the exceptionally well-dated Soreq cave records, now allows studying older sapropels with much better time constraint (Grant et al., 2012, 2016). Sapropel S3 (~85.8–80.8 kyr BP) was deposited at a time of glacial inception when ice sheets were growing (e.g. Waelbroeck et al., 2002) and sea level was ~30–40 m lower than at present and ~25 m lower than during S1 (Grant et al., 2012, 2016). At the same time S3 experi-enced a somewhat higher Northern Hemisphere summer insola-tion compared to S1, which is thought to be associated to a stronger North African monsoon intensity (e.g. Emeis et al., 2003).

While summer monsoons may have been enhanced during S3, pollen records point to more arid and cooler mean annual climate in the Eastern Mediterranean Sea area during S3 relative to S1 (Cheddadi and Rossignol-Strick, 1995a; Langgut et al., 2011; Langgut, 2017), in line with a glacial climate mode. The multiple (high resolution) palynological records for sapropel S1 (e.g. Rossignol-Strick et al., 1982; Rossignol-Strick, 1999; Zonneveld et al., 2001; Sangiorgi et al., 2003; Kotthoff et al., 2008; Langgut et al., 2011; van Helmond et al., 2015) indicate that enhanced summer monsoon-driven freshwater input accompanied sapropel formation, mostly favouring the development of anoxia through water-column stratification, as marine productivity alone already increased before sapropel deposition (van Helmond et al., 2015). At present, high-resolution studies of S3 are virtually missing. None-theless, these are essential to fully understand the different pro-cesses (e.g. Nile discharge, productivity, water column processes, and bottom-water redox conditions) leading to S1 and S3 deposition.

Here we present a high-resolution palynological, i.e. organic-walled dinoflagellate cysts (dinocysts) and pollen/spores, and geochemical (trace elements) record for sapropel S3 and compare it to S1 from the same sediment record, ~150 km offshore the Nile (Fig. 1). We reconstruct (1) a marine signal related to Mediterra-nean surface waters using dinocysts, (2) a terrestrial vegetation and runoff signal using pollen and palynomorphs related to the Nile catchment area, and (3) water column processes and sediment anoxia recorded in the sediment from geochemical data.

2. Material & methods

2.1. Sample material

Piston core MS21PC (32°20.7′N, 31°39.0′E; 1022 m water depth; 752 cm in length) was retrieved from the central Nile cone during
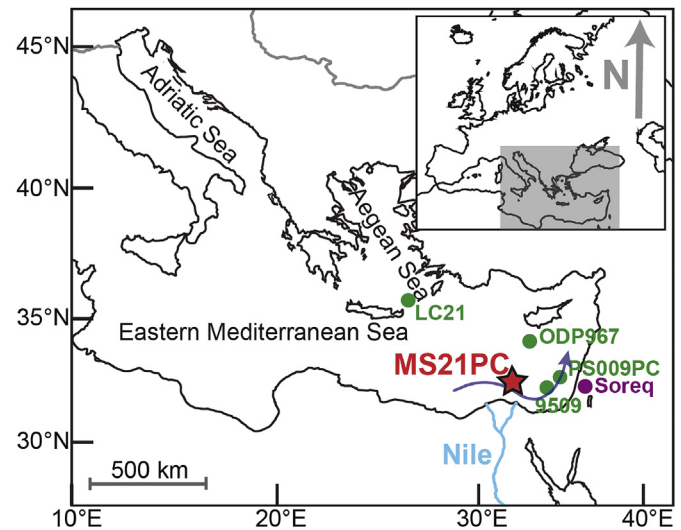
Fig. 1. Location of core MS21PC (32°20.7′N, 31°39.0′E; 1022 m water depth) in the Eastern Mediterranean Sea (Red Star). The Soreq cave (e.g., Bar-Matthews et al., 2003) is indicated with purple. Marine cores LC21 (e.g., Grant et al., 2016), ODP967 (e.g., Emeis et al., 2003), PS009PC (Hennekam et al., 2014; van Helmond et al., 2015), and 9509 (e.g., Matthews et al., 2017) are indicated with green. Dark blue arrow indicates the prevailing currents around the Nile delta. (For interpretation of the references to colour in this figure legend, the reader is referred to the Web version of this article.)

the MIMES cruise with *R/V Pelagia* in 2004 (Fig. 1). The sediments primarily consist of grey-brown clays, dominated by Nile-derived smectites (~70%; Venkatarathnam and Ryan, 1971). Sapropel sedi-ments occur at respectively ~35–95 (S1) and ~605–660 (S3) cm below sea floor (cmbsf).

2.2. Age model

The age model for the top ~30 kyr in core MS21PC is constrained by 6 previously published radiocarbon dates (Hennekam et al., 2015a), complemented by 3 new radiocarbon dates (Table 1, Fig. 2a). Radiocarbon analyses were done on 10 mg of mixed planktic foraminifer material at the Poznań Radiocarbon Laboratory in Poland. The part of the core that fell outside the ^{14}C window was dated by tuning of the surface-dwelling planktic foraminifer *Glo-bigerinoides ruber* oxygen isotope ($\delta^{18}O_{ruber}$) record to the $\delta^{18}O$ re-cord of the Soreq Cave speleothems ($\delta^{18}O_{speleo}$), following Grant et al. (2012). The moisture source of the Soreq Cave speleothems is mainly Eastern Mediterranean Sea surface water and therefore variability in $\delta^{18}O_{speleo}$ co-varies with $\delta^{18}O_{ruber}$ via the "source ef-fect". This approach allows the transference of the exceptionally well-dated Soreq Cave chronology (Bar-Matthews et al., 2003) to Mediterranean sediments (Grant et al., 2012, 2016). We also chose one tie-point to the LC21 $\delta^{18}O_{ruber}$ record (Grant et al., 2012). This

Table 1
The ^{14}C data used to construct the age model for MS21PC.

Depth (cm)	[14]C age (yr BP) ± 2σ	[14]C lab code	Reference
18.5	3640 ± 40	Poz-55166	Hennekam et al., 2015a
38.5	6330 ± 50	Poz-55167	Hennekam et al., 2015a
58	7850 ± 50	Poz-55168	Hennekam et al., 2015a
86	9110 ± 50	Poz-55169	Hennekam et al., 2015a
121	10540 ± 50	Poz-55170	Hennekam et al., 2015a
142	11860 ± 70	Poz-55172	Hennekam et al., 2015a
169.5	14730 ± 60	Poz-55173	This study
200.5	18950 ± 100	Poz-55174	This study
264.5	26740 ± 190	Poz-55176	This study
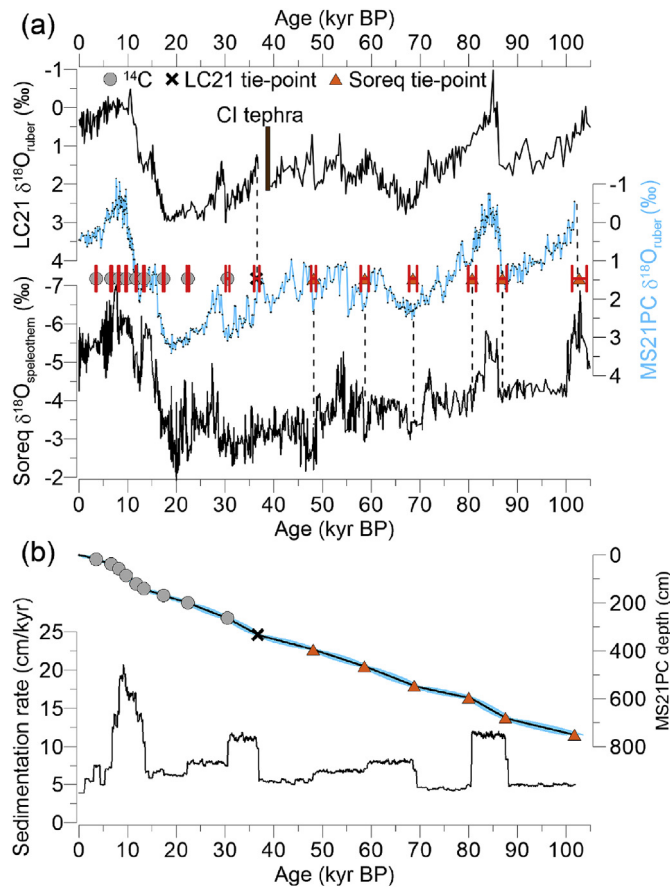
Fig. 2. (a) Tuning of core MS21PC $\delta^{18}O_{ruber}$ (this study) to LC21 $\delta^{18}O_{ruber}$ and Soreq $\delta^{18}O_{speleothem}$ (see also Rohling et al., 2017). The ^{14}C dating points (circles), Soreq-MS21PC tie-points (triangles), and MS21PC-LC21 tie-point (cross) and their error margins (2σ, red bars) are indicated. Brown bar indicates Campanian Ignimbrite-tephra horizon in the LC21 record of Grant et al. (2012), used for the MS21PC-LC21 tie-point. The Soreq-MS21PC tie-points are used to transfer the well-dated Soreq cave chronology (Bar-Matthews et al., 2003; Grant et al., 2012) to the MS21 record. (b) Age-depth model including the minimal-maximum error margins (blue shading) and sedimentation rate through time of core MS21PC, both calculated with the Bacon program of Blaauw and Christen (2011). The $\delta^{18}O_{ruber}$ values for the first 13 kyr (n = 277) were published in Hennekam et al. (2015a). (For interpretation of the references to colour in this figure legend, the reader is referred to the Web version of this article.)

tie-point at 36.48 ± 0.55 kyr BP is close to the Campanian Ignimbrite-tephra horizon in the LC21 record, and can thus be regarded as a robust dating point, which we transferred to our record.

The final age model was generated using a Bayesian deposition model, calculated with the 'Bacon' software package for R (Blaauw and Christen, 2011), including all radiocarbon and tie-point ages and their corresponding uncertainties (Fig. 2b). The age model parameters were chosen based on recommendations in Blaauw and Christen (2011) for an environment with low "memory" in accumulation rates (i.e. acc.shape = 2, mem.strength = 20, mem.-mean = 0.1). The Marine '13 curve was used for calibration of our radiocarbon-dated samples performed within the Bacon program. We used a local reservoir correction (ΔR) of 21 ± 63 yrs outside the sapropel S1 interval, based on ^{14}C analyses of recent shell material in proximity of the core (Boaretto et al., 2010; Reimer and McCormac, 2002), and 149 ± 30 yrs within the sapropel period (Facorellis et al., 1998; Grant et al., 2012).

2.3. Geochemical procedures and analyses

Core MS21PC was analysed with a 0.5—2 cm resolution for total organic carbon (C_{org}) by thermal combustion after removal of $CaCO_3$ from freeze-dried sediment samples by HCl extraction. Measurements (n = 360) were performed with a Fisons NA1500 NCS analyser at Utrecht University. During the measurements in-house reference material (nicotinamide; N = 45) showed precision (relative standard deviation) of <2% and accuracy (% deviating from reference value) < 1%.

Aliquots of dried sediment samples were also digested with an $HClO_4$—HNO_3—HF acid mixture and subsequently measured for aluminium (Al), phosphorus (P), sulphur (S), manganese (Mn), barium (Ba), and molybdenum (Mo) by Inductively Coupled Plasma-Optical Emission Spectroscopy (ICP-OES; 437 samples) and for uranium (U) and Mo by ICP-Mass Spectrometry (ICP-MS; 102 samples) in a 0.5—2 cm resolution (for details see Hennekam et al., 2015b). These measurements were performed with a Spectro Ciros Vision ICP-OES and Thermo Scientific X-Series 2 ICP-MS, both at Utrecht University. Reference material (ISE-921) showed accuracies <5% for Al, P, S, Mn, and Ba, and <7% for U. No reference value is available for Mo in the ISE-921 standard, but the ICP-OES and ICP-MS measurements showed an average difference <13%. The precision (relative standard deviation) was <5% for all elements.

The $\delta^{18}O_{ruber}$ were measured as described in Hennekam et al. (2015a). For this study the existing dataset (~13 kyr interval; n = 277) was extended to the base of the core (adding 318 samples). The measurements were performed on a Finnegan MAT-253 mass spectrometer, connected to a Kiel-III carbonate preparation device. The $\delta^{18}O$ (in ‰ relative to the Vienna PeeDee Belemnite, VPDB) was measured on an aliquot of a crushed sample existing of ~20—30 G. ruber tests. In all samples, G. ruber (white) were picked from the 250—300 μm size range. NBS-19 standards were frequently measured within each run, showing an average standard deviation of ~0.06‰.

2.4. Palynological procedures and analyses

Seventy-five samples were prepared for palynological analysis, following standardized quantitative methods used at the Laboratory of Palaeobotany and Palynology, Utrecht University, The Netherlands. For sapropel S1, 19 samples were selected between 19.5 and 105.5 cmbsf, yielding an average sample resolution of 4.5 cm (multi-centennial). For sapropel S3, 56 samples were selected between 589.75 and 695 cmbsf, yielding an average sample resolution of 1.9 cm (multi-decadal to centennial). Between 0.99 and 2.47 g of freeze-dried sediment was gently crushed and a tablet containing a known amount of Lycopodium clavatum spores was added to enable quantification of palynomorph concentrations (palynomorphs/gram dry sediment) following Wood et al. (1996). Subsequently, samples were treated with 10% HCl and 38% HF, to dissolve carbonates and silicates, respectively. The residue was then sieved over a 10-μm sieve after which the concentrated residue was mounted onto microscope slides.

Dinocysts, other aquatic palynomorphs, pollen and spores were identified to, when possible, species level using an Olympus CX21 light microscope at 400× magnification. Dinocyst taxonomy follows Rochon et al. (1999) and Fensome and Williams (2004). Pollen taxonomy follows Beug (2004) and Reille (1992). On average, 197 dinocysts per sample were counted, with a minimum count of 99 in pre-sapropel S3 samples. On average, 364 pollen were counted per sample, pre-sapropel S3 sample counts of <50 grains are considered not reliable (indicated in Fig. 5). Percentages of dinocyst species and pollen were calculated on a sum of total dinocysts and total pollen, respectively. Palynomorph accumulation rates were also

calculated dividing the palynomorph concentration by the sediment accumulation rates (g cm^{-2} yr^{-1}).

2.5. Geochemical proxies

The $\delta^{18}O_{ruber}$ depends on isotopic fractionation related to temperature and the isotopic composition of the surface seawater. The latter, in turn, mainly depends on global ice volume and evaporation/precipitation (e.g. Rohling and Bigg, 1998). The Nile river is known to have a profound influence on the Mediterranean surface water $\delta^{18}O$, especially during sapropel formation (e.g. Fontugne et al., 1994; Rohling and De Rijk, 1999; Emeis et al., 2003; Hennekam et al., 2014). A depleted $\delta^{18}O$ signal is particularly recorded in the carbonate of the planktic foraminifer *G. ruber*, which can inhabit freshwater lenses (Rohling et al., 2004). As such, negative excursion in $\delta^{18}O_{ruber}$ dominantly relates to North African (Nile) runoff during sapropel deposition. However, the Mediterranean is a restricted basin with a relatively shallow connection to the open ocean at Gibraltar and therefore a strong sea level-related concentration effect on Mediterranean $\delta^{18}O$ over glacial-interglacial timescales (Rohling, 1999; Rohling et al., 2014, 2017; Grant et al., 2016). It is therefore likely that the enhanced ice volume effect significantly enriches $\delta^{18}O_{ruber}$ during S3 relative to S1. To effectively correct for this sea level component in the $\delta^{18}O_{ruber}$ signature, we adopt the method of Rohling et al. (2014) and Grant et al. (2016), which used the Red Sea relative sea-level record, and calculate residual $\delta^{18}O_{ruber}$ values for our MS21PC record ($\delta^{18}O_{residuals}$). Here, we focus on the $\delta^{18}O_{residuals}$ that are more negative than the 1σ (most depleted) confidence limit, to assess differences in Nile discharge during sapropels S1 and S3.

Barium enrichment in sediments is linked to biogenic Ba ($BaSO_4$) precipitation in the water column associated with decaying organic matter and is, therefore, regarded as a proxy for export-productivity (e.g. Bishop, 1988; Dymond et al., 1992). This association for Ba appears to work particularly well for Mediterranean sapropels, being relatively resistant to diagenesis, especially in comparison to C_{org}, which is easily respired after deposition ('burn-down') in the presence of oxygen (Van Santvoort et al., 1996; Weldeab et al., 2003). We present Ba (and other elements) as concentrationtrations and normalized as a ratio to Al to avoid closed-sum effects through variability in carbonate content (Thomson et al., 1999).

The redox state dependency of Mo, S, U, Mn, and total organic carbon/total phosphorus (C_{org}/P_{tot}) can be used to define the strength of anoxia during sapropels S1 and S3 (e.g. Tribovillard et al., 2006; Algeo and Ingall, 2007; Scott and Lyons, 2012). Immobilization of Mn, U, and Mo in the sediment occurs along a distinct oxic to sulfidic gradient (e.g. Tribovillard et al., 2006). Specifically, elevated sedimentary Mo concentrations are associated with euxinic conditions in bottom- and/or pore waters, as Mo is scavenged in the presence of free sulfide (H_2S; Helz et al., 1996), while similarly S concentrations relate to pyrite formation under sulfate-reducing conditions (e.g. Passier et al., 1999). Uranium uptake into the sediment commences around the Fe-reduction boundary (Algeo and Tribovillard, 2009; Tribovillard et al., 2012) and therefore starts to be enriched in the sediment under sub-oxic conditions. The C_{org}/P_{tot} ratio can also be used to indicate low oxygen conditions, because P regeneration enhances when Fe-oxyhydroxides are reduced (e.g. Slomp et al., 2002; Algeo and Ingall, 2007; Kraal et al., 2010). In contrast, Mn is remobilized as Mn^{2+} forms as a reaction product of Mn-oxyhydroxide reduction in sediments. As such, Mn is generally low in sapropels and is only diagenetically enriched upon reventilation at the end of sapropel formation and subsequently downward progressing oxidation front into the sapropel sediments (Van Santvoort et al., 1996; De Lange et al., 2008). In short, Mo, S, U, and C_{org}/P_{tot} generally increase during low-oxygen conditions in bottom water and/or sedimentary pore waters (e.g. during sapropels), while Mn is lower during these intervals and increases during oxygenation/reventilation.

2.6. Palynological proxies

The total dinocyst accumulation rate (number of cysts cm^{-2} yr^{-1}) is considered to be a good proxy for surface water primary productivity (Zonneveld et al., 2009). Also the ratio between heterotrophic and autotrophic (H/A-ratio) dinocysts has been used as an indicator for primary productivity (e.g., Sangiorgi and Donders, 2004). Certain dinocyst species are, however, more resistant to aerobic decay than others. Heterotrophic dinocysts are in general more prone to oxidation in well-oxygenated environments (Zonneveld et al., 2001; Versteegh et al., 2010; Gray et al., 2017). Therefore, when redox conditions vary, for example between sapropel and non-sapropel intervals, selective preservation of dinocysts may bias paleoenvironmental reconstructions based on these assemblages. We therefore also separately considered the accumulation rates of dinocysts resistant to aerobic decay (*Operculodinium centrocarpum/israelianum*, *Pentapharsodinium dalei*, *Impagidinium* spp. and *Polysphaeridium zoharyi* in our samples) to aid interpretations of productivity patterns.

A selected number of dinocyst species is used in this study for environmental interpretations. Heterotrophic dinocysts, particularly *Brigantedinium* spp., are generally abundant in high productivity, high nutrient environments (e.g., De Vernal and Marret, 2007; Zonneveld et al., 2013). Dinocysts belonging to the genus *Impagidinium* are mostly present in temperate, oligotrophic open waters; *Lingulodinium machaerophorum* is abundant in coastal regions and regions in the vicinity of continental margins. High relative abundances are observed in sediments near upwelling cells or below river plumes (Sangiorgi and Donders, 2004), in seasonally stratified, nutrient-rich environments. *Spiniferites* spp. is cosmopolitan, while *Tuberculodinium vamcampoae*, at present a relatively uncommon species, found in coastal embayment, is most abundant (~30%) in warm temperature to equatorial areas (Zonneveld et al., 2013 and references therein).

The terrestrial/marine ratio (T/M ratio) shows the ratio between the amount of terrestrial (pollen and spores) and marine (dinocysts) palynomorphs in the samples. This ratio is used as an indicator for riverine input. Due to more efficient long-distance transport (Mudie, 1982; Heusser, 1983), better preservation of bisaccate pollen (Cheddadi and Rossignol-Strick, 1995b), and potential variations in Nile outflow rate and location in the delta (Hennekam et al., 2015a), percent abundances of individual taxa are based on a sum of total pollen and spores excluding bisaccates. This is to avoid transport and preservation bias on the interpretations.

Studies in different marine settings show that relative pollen composition in marine sediments close to rivers primarily reflects vegetation types in the river's catchment area and that the majority of pollen are transported by water (Heusser, 1983; Moss et al., 2005; Dai et al., 2014). Regional vegetation types surrounding the Eastern Mediterranean, summarized by Langgut (2017), that provide the principal sources for the key pollen types are the Mediterranean (*Quercus, Pinus,* and *Rumex*), Irano-Turanian semi desert (Poaceae and Chenopodiaceae, and *Artemisia*), and Saharo-Arabian desert types (*Artemisia,* Poaceae, Chenopodiaceae, and *Ephedra*) (Cheddadi and Rossignol-Strick, 1995b; Langgut et al., 2011). The desert type, especially Chenopodiaceae, can also represent coastal halophytic vegetation. Cyperaceae represent largely marsh environments associated with river banks and deltas (Bernhardt et al., 2012). An eastward shift in the Cyperaceae abundance during S1, i.e. from site MS21PC to PS009PC, is interpreted by Hennekam et al. (2015a) as

an eastward shift of Nile outflow. Spore (particularly trilete) abundances have been used previously to trace the relative input of upland erosion (see e.g. Langgut, 2017 and references therein) as spores originating from deltic sources are generally limited. Trilete spore abundances elevated prior to S1 and S3 can be explained by vegetation cover decline and erosion of Ethiopian Jurassic deposits during dry phases (Langgut, 2017). Tropical elements from the upper Nile reaches are typically limited due to degradation during transport and relatively low pollen production, while deciduous mesophytic elements (e.g. *Corylus, Carpinus, Ostrya*) most likely represent long distance transport from northern Mediterranean sources (see Langgut, 2017).

Other aquatic palynomorphs were counted and identified. In particular, two freshwater (freshwater-tolerant) green algae species, *Pediastrum* spp. and *Staurastrum* spp. are used to detect freshwater input and grouped together as 'fresh and brackish water palynomorphs'.

3. Results

3.1. Geochemistry

The large-scale trends in C_{org}, Ba(/Al), S, Mo(/Al), U(/Al) and C_{org}/P_{tot} are similar in both sapropels S1 and S3, with increased values during the sapropels (Fig. 3b–g). In contrast, Mn(/Al) is low within the sapropels (Fig. 3h). Within sapropel S1 at ~8 kyr BP, a spike in Mn/Al is visible, concurrent with minor troughs in C_{org}, Ba(/Al), Mo(/Al) and C_{org}/P_{tot} (Fig. 3), splitting the sapropel in two halves (i.e. S1a and S1b, cf. De Rijk et al., 1999). Maximum values for S, Mo(/Al), and C_{org}/P_{tot} are higher in S3 relative to S1. The C_{org} in S3 is similar to that of the first half of S1 (S1a), and higher than the values observed in the second half of S1 (S1b), whereas Ba(/Al) values are comparable. U(/Al) values are generally similar throughout, with

the exception of S1b where values are higher.

Prior to both S1 and S3 the $\delta^{18}O_{ruber}$ decreases to average values of −0.39‰ and 0.00‰, respectively, within the sapropels (Fig. 3a). For both sapropels the minimum $\delta^{18}O_{ruber}$ is found halfway through the sapropel and then slowly increases towards ~0.40‰ at ~3 kyr BP for S1 and ~1.00‰ at ~78 kyr BP for S3.

3.2. Palynology: dinocysts and other aquatic palynomorphs

Both S1 and S3 contain abundant and well-preserved dinocysts (see Fig. 3 and Fig. 4 of supplementary data). In both sapropels the assemblages are dominated by *Brigantedinium* spp., *Impagidinium* spp., *Lingulodinium machaerophorum*, *Spiniferites* spp. (Fig. 4d–g), *Operculodinium* spp. and cysts of *Pentapharsodinium dalei*. In addition, Sapropel S3 contains abundant *Tuberculodinium vancampoae* (Fig. 4h), reaching maximum values up to 30% and accumulation rates of 16 cysts $cm^{-2}yr^{-1}$ during its early stages. *L. machaerophorum* is more abundant in S3 relative to S1, reaching peaks of 40% and 14%, respectively, and has much higher accumulation rates. Dinocyst assemblages in the lower part of S3 are dominated by *Spiniferites* spp. and *T. vancampoae*, while *Brigantedinium* spp. and *L. machaerophorum* mostly increase in the upper part.

Dinocyst accumulation rates (number of cysts cm^{-2} yr^{-1}) increase to maximum values of 30 cysts cm^{-2} yr^{-1} in the first half of S1 at 8.9 kyr BP, and then markedly drop to pre-sapropel values in the second half of sapropel S1, starting around 8.4 kyr BP (Fig. 4b). Dinocyst accumulation rates start to increase gradually approximately 2 kyr before the onset of sapropel S3, at ~88 kyr BP (Fig. 4b). A more rapid increase occurs within the sapropel, where dinocyst accumulation reaches values of ~74 cysts cm^{-2} yr^{-1} and decreases again after the sapropel termination. The accumulation rates of dinocysts resistant to aerobic decay (Fig. 4b) generally mirror that
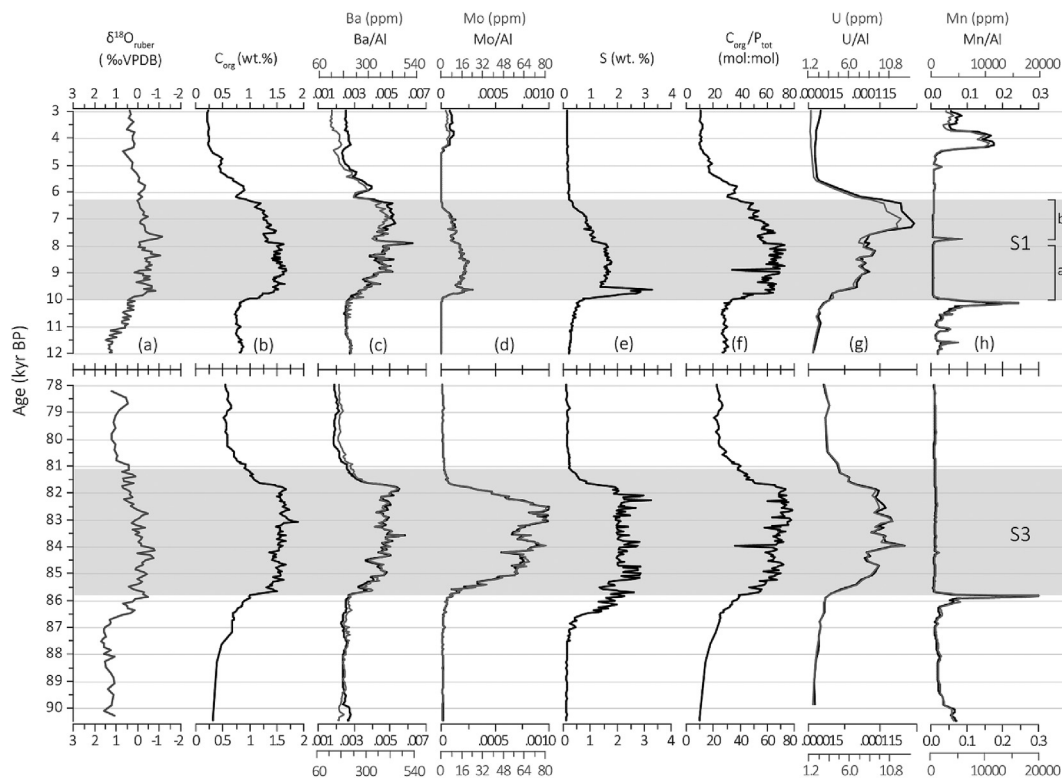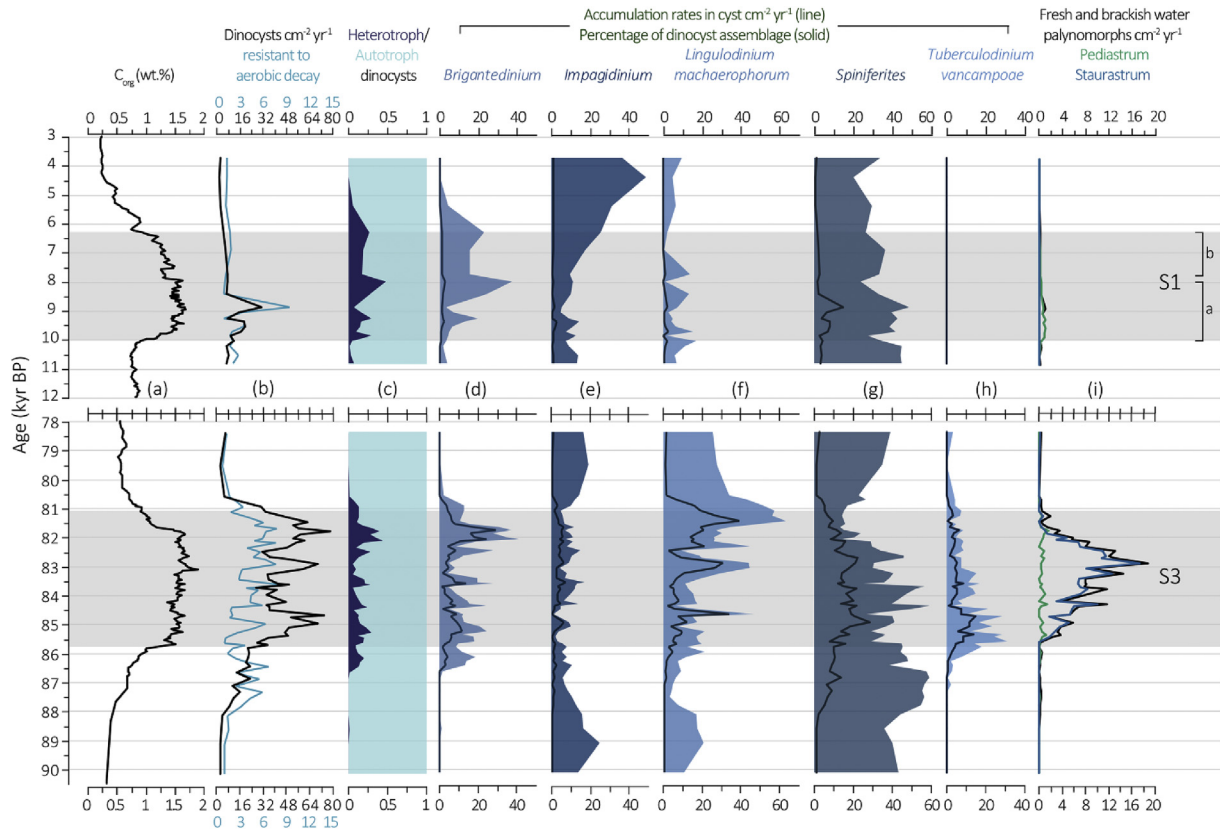

Fig. 3. Sediment geochemistry plotted against age. (a) $\delta^{18}O_{ruber}$. (b) C_{org} weight percentages. (c) Ba/Al and Ba in ppm. (d) Mo/Al and Mo in ppm. (e) S weight percentages. (f) $C_{org}:P_{tot}$. (g) U/Al and U in ppm. (h) Mn/Al and Mn in ppm.

Fig. 4. Relative and absolute dinocyst abundances plotted against age. (a) C_{org} weight percentages. (b) Total dinocyst accumulation rates in cyst per cm^2 yr^{-1} in black and those resistant to aerobic decay in light blue. (c) Heterotroph/Autotroph ratio. (d) *Brigantedinium,* silhouette represents relative abundanceof the total assemblage, line shows accumulation rate in cyst per cm^2 yr^{-1}, which is the same for (e) *Impagidinium*, (f) *Lingulodinium machaerophorum*, (g) *Spiniferites* and (h) *Tuberculodinium*. (i) Fresh and brackish water palynomorphs in palynomorph per cm^2 yr^{-1}. Total is shown in black, green shows *Pediastrum* and blue indicates *Staurastrum* spp. (For interpretation of the references to colour in this figure legend, the reader is referred to the Web version of this article.).

of the total dinocysts, particularly in S1.

In S1, the H/A ratio is somewhat higher at the onset than at the end of the sapropel. The H/A ratio reaches its maximum value of 0.47 around 8 kyr BP (Fig. 4c). In S3 the H/A ratio starts to increase around 86.5 kyr BP, which is ~1 kyr before the onset of sapropel formation, the maximum value of 0.43 in S3, following gradual increase is reached around 82 kyr BP (Fig. 4c).

The remains of the freshwater-tolerant green algae *Pediastrum* spp. occur within and before both sapropels (Fig. 4i), being most abundant within S3. Another freshwater palynomorph, the green algae *Staurastrum* spp., is very abundant in S3, while it is only found once in S1. The combined accumulation rates of fresh and brackish water species show highest abundances within S3.

3.3. Palynology: pollen and spores

Similar to the dinocysts, the pollen accumulation rates in S1 are highest in the first half of the sapropel, reaching up to 100 pollen cm^{-2} yr^{-1} (Fig. 5b) in all types, except for *Artemisia* and bisaccates. In S3 pollen accumulation rates rapidly increase from ~86.5 kyr BP, maintaining high values (on average 94 pollen cm^{-2} yr^{-1}, up to 144 cm^{-2} yr^{-1}) throughout S3 after which they decrease abruptly at the end of the sapropel. Accumulation rates start to increase 0.5−1 ka before visible sapropel deposition (Fig. 5b), which is mirrored in the ratio between terrestrial and marine palynomorphs (T/M ratio). The T/M is highest within the sapropel with values between ~0.5 and 0.75 in both S1 and S3 (Fig. 5c). Concurrent with the change in C_{org} (Fig. 5a), post-sapropel the T/M values return to just below 0.5

for S3 and below 0.25 for S1.

Pollen assemblages in both sapropels are dominated by *Pinus*, Asteraceae, *Artemisia,* Chenopodiaceae*,* Cyperaceae, Poaceae, *Quercus robur*-type *(deciduous)* and *Q. ilex*-type *(evergreen)*, *Rumex*, and *Ephedra fragilis* (Fig. 5e−k; also Fig. 1 and Fig. 2 of supplementary data). Angiosperm and herb pollen abundances (Fig. 5d) decrease gradually during S1, causing the proportion of *Pinus* to reach over 60% of the total assemblage right after S1 termination. This increase is a result of the closed-sum effect, because the *Pinus* influx remains more or less stable (Fig. 5d). Relative to S1, bisaccate pollen percentages during S3 are stable and low (12−24%; Fig. 5d). During S1, total angiosperm tree pollen are relatively high (11−28%), and predominantly consist of *Quercus* (mostly *Q. robur* type). In contrast, the pollen assemblages in S3 are dominated by herbs (75−87%), while angiosperm tree pollen are much less abundant (8−19%). Total *Quercus* increases pre-sapropel in both S1 and S3, reaching maxima of 25% (S1) and 14% (S3) within the sapropel (Fig. 5i). Post-sapropel decrease is clear in S3, while S1 *Quercus* values fluctuate but do not decline. Evergreen oak pollen (*Q. ilex*-type) are infrequent (<2.5%) but occur mainly during sapropel formation (Fig. 5i), with a small but pronounced maximum during the second half of S1, while *Q. cerris* type is low throughout. The dominant herb taxon *Artemisia* represents 20−35% of the assemblages during sapropel S3, and decreases to 10% pre and post sapropel, while Cyperaceae and Poaceae gradually increase. The increase in *Artemisia*, from ~3 to 10%, is much less pronounced in S1, although other Asteraceae are relatively higher. In S1, *Artemisia* occurs mainly during the second half. In both S1 and S3,
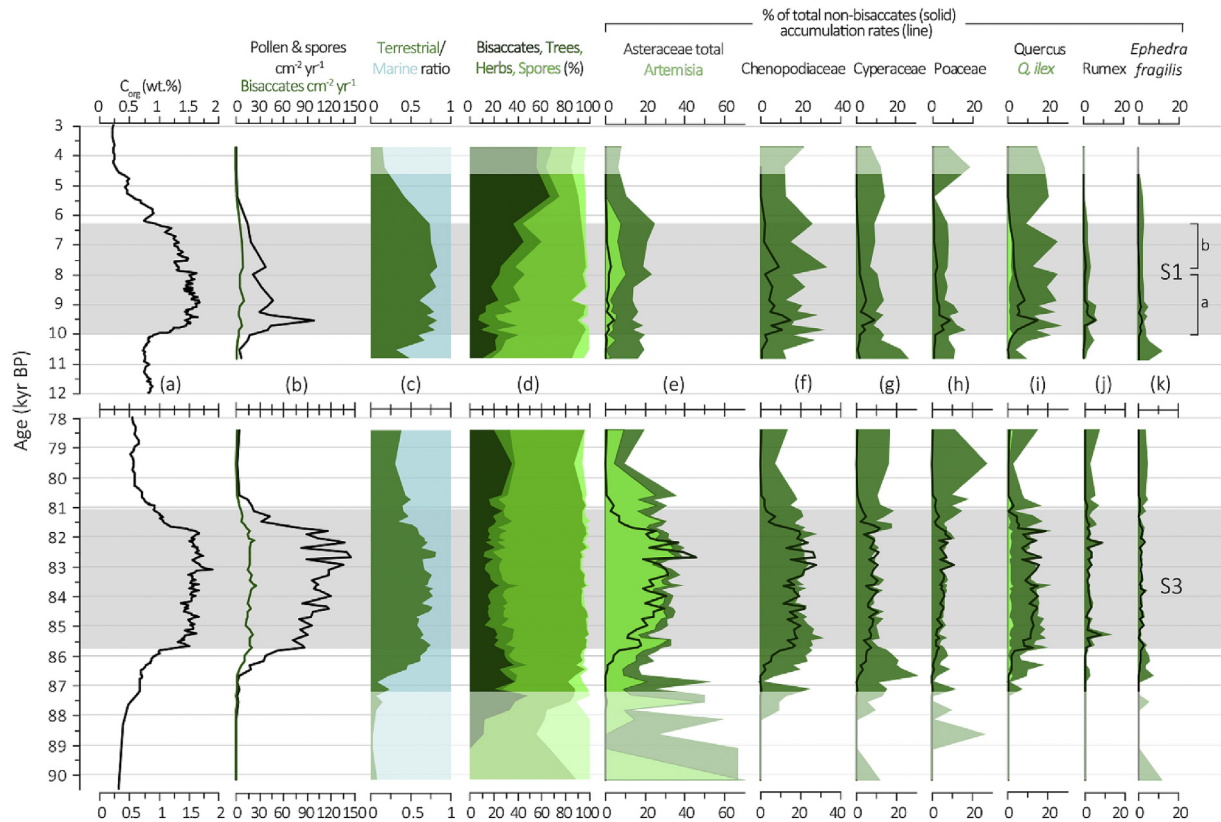
Fig. 5. Relative and absolute pollen and spore abundances plotted against age. (a) C_{org} weight percentages. (b) Total pollen and spores accumulation rates in palynomorphs per cm^2 yr^{-1} (black line) and total bisaccates green line. (c) Terrestrial/Marine ratio. (d) Total pollen and spore assemblage in percentages, bisaccates in dark green, followed by trees, herbs and spores in the lighter greens. (e) Asteraceae with *Artemisia*-type overlay in light green, silhouettes represent the relative abundance of the total pollen and spore assemblage excluding bisaccates, black lines show accumulation rates in pollen per cm^2 yr^{-1}, which is the same for (f) Chenopodiaceae, (g) Cypercaceae, (h) Poaceae, (i) *Quercus* with *Q. ilex* overlay in light green, (j) *Rumex*, and (k) *Ephedra fragilis*. Low count sums (<50 pollen and spores) pre-S3 and post-S1 are indicated by light shading and considered not reliable (see section 2.4). (For interpretation of the references to colour in this figure legend, the reader is referred to the Web version of this article.)

Chenopodiaceae increase from 6 to 20–30% prior to and during the early stages of the sapropel and decrease after sapropel termination. *Ephedra fragilis* shows somewhat higher abundances prior to (S1 and S3) and post-sapropel (S3) deposition. In S1 a maximum in *Rumex* is observed during the early stages of S1, while such distinct maximum is absent for S3. Relative spore abundances are elevated prior and post S3, but the input of resistant spores remains relatively low and stable. Influx of trilete spores, previously suggested to represent dry phase upland erosional signals (Langgut, 2017), shows a minor increase during sapropel S3 deposition, between ~81 and 85 ka (Fig. 2, supplementary data).

4. Discussion

Recent attempts to objectively assess sapropel boundaries have used the shape of C_{org}, Ba/Al, and Mn/Al profiles over depth (e.g. De Lange et al., 2008). Accordingly, we use the increase and decrease in C_{org} content (~1–1.5% maximum), as compared to pre- and post-sapropel sediments (~0.5%), and the sharp increase/decrease of Ba/Al, which is known to be less prone to post-depositional diagenesis compared to C_{org} (Van Santvoort et al., 1996; Thomson et al., 1999). Nonetheless, productivity and reduced seafloor oxygen concentrations were possibly present well outside the interval of these sapropel boundaries (e.g. Grimm et al., 2015; van Helmond et al., 2015; Grant et al., 2016). Below we use the palynological and geochemical sedimentary data to describe (1) Nile river discharge, (2) vegetation variability in and around the Nile catchment, (3) marine productivity signals, and (4) sedimentary and water-

column redox conditions prior to, during and after sapropels S1 and S3.

4.1. Nile river discharge

The increased inflow of depleted-$\delta^{18}O$ (Nile) water is clearly recorded in the $\delta^{18}O_{ruber}$ for sapropels S1 and S3. The $\delta^{18}O_{ruber}$ in the Mediterranean is known to be influenced by enhanced precession-driven North African monsoon intensity and related freshwater discharge during sapropel times (e.g. Rossignol-Strick, 1985), particularly in the Nile delta area (e.g. Fontugne et al., 1994; Hennekam et al., 2014). After correction for the glacial concentration effect in the Mediterranean basin (see section 2.5; Rohling et al., 2014; Grant et al., 2016), the $\delta^{18}O_{residuals}$ for S1 and S3 indicate average values of −0.85‰ and −0.92‰, respectively (Fig. 6a). The corrected values thus suggest freshwater input and a stronger Nile discharge during sapropel S3 relative to S1, at least at this core location.

Intensified Nile discharge during deposition of both sapropels is further supported by the higher T/M ratios and corresponding total pollen and spores accumulation rates (Fig. 6b and c) and the higher sedimentation rates during sapropel formation (Fig. 2b). The T/M ratio is impacted by closed-sum effects and could be biased by higher preservation during the sapropels and differential preservation between marine and terrestrial palynomorphs (McCarthy et al., 2003). Therefore the T/M ratio might be less indicative of true magnitude differences of Nile discharge. Nevertheless, the T/M ratio profiles quite closely mimic — and thereby confirm — the
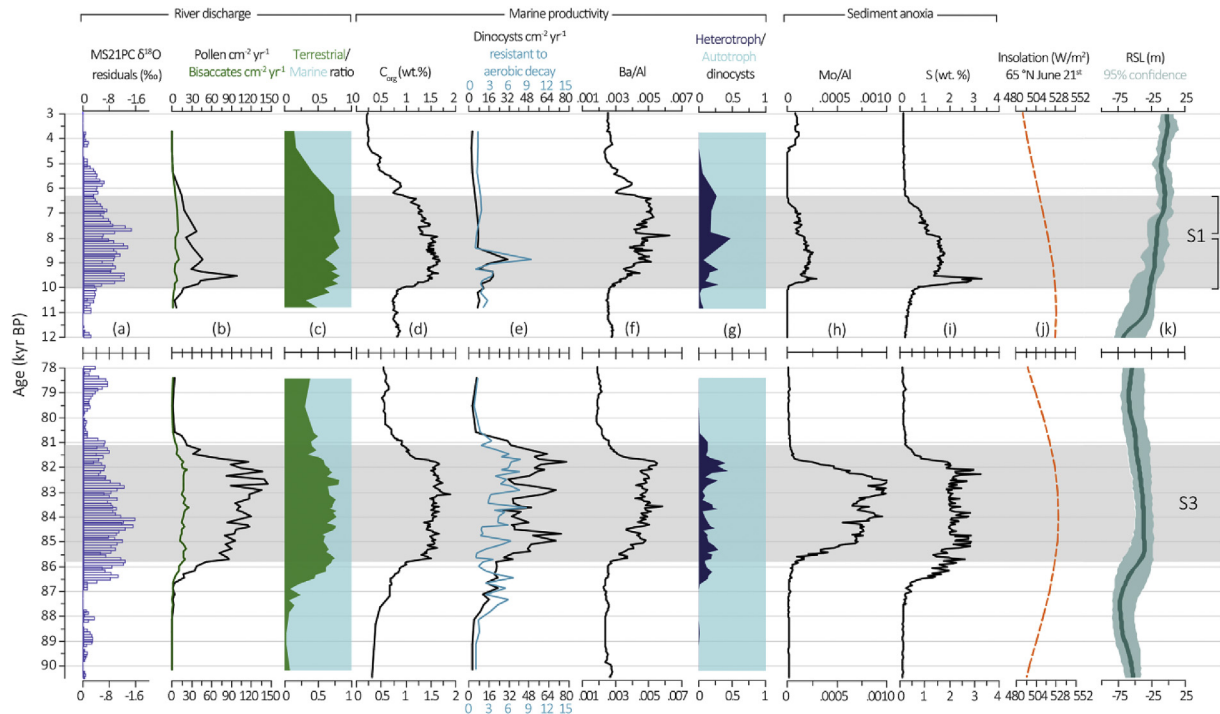
Fig. 6. Overview of selected palynological and geochemical data. (a) $\delta^{18}O_{residuals}$ (calculations following Rohling et al., 2014 and Grant et al., 2016, see Methods). (b) Total pollen and spores accumulation rates, with bisaccates in green. (c) Terrestrial/Marine ratio. (d) C_{org} weight percentages. (e) Dinocyst accumulation rates, including those resisting to aerobic decay in blue. (f) Ba/Al. (g) Heterotroph/Autotroph ratio. (h) Mo/Al. (i) S weight percentages. (j) Insolation (W/m^2) 65°N, 21st of June (Laskar et al., 2004). (k) Red Sea relative Sea Level (RSL) in meters in dark blue, 95% confidence level in light blue (Grant et al., 2012). (For interpretation of the references to colour in this figure legend, the reader is referred to the Web version of this article.)

$\delta^{18}O_{residuals}$ profiles, showing a relative increase in the influx of pollen and spores during and after both sapropels, and a lower level before sapropel deposition.

Both $\delta^{18}O_{residuals}$ and the T/M ratio indicate that Nile discharge increased at least ~1 kyr before both sapropels. The observed trends in Nile runoff are further supported by the relative abundances of bisaccate pollen (Fig. 5d). Bisaccate pollen are generally well represented in marine sediments, because they are easily transported over long distances by wind and rivers and because they are relatively resistant to degradation (Cheddadi and Rossignol-Strick, 1995b; McCarthy et al., 2003). This makes bisaccate pollen especially dominant during low river outflow, but less dominant when river discharge increases. Sapropel S1 registers a high river discharge at its onset and during deposition of its lower part, and subsequently a gradually decreasing river input. In S3, bisaccate percentages are clearly lowest within the sapropel, which is in good agreement with a strong river input as suggested by T/M ratios and $\delta^{18}O_{residuals}$ during this time.

Other indicators of a strong riverine influence are the brackish and freshwater algae species present predominantly in S3 (Fig. 4i). The most abundant are the green algae *Staurastrum* spp. and *Pediastrum* spp. The latter can be seen as a direct signal for the presence of freshwater (Head, 1993). *Straurastrum* spp. was previously found in sediments from Canadian lakes (Danesh et al., 2013) and is uncommon in marine sediments. It has been found in the inner shelf and delta front region of the Arctic Ocean (Matthiessen et al., 2000). Its presence in a marine record clearly signals a strong influence of the river Nile during S3, confirming higher Nile discharge during S3 relative to S1. Increasing relative abundances and accumulation rates of *Lingulodinium machaerophorum* during S3 (Fig. 4f) further confirm high riverine input as this species is found in high abundances in river plume areas, in seasonally

stratified waters, during periods with high nutrient input (Zonneveld et al., 2013). In S1 *L. machaerophorum* abundances and accumulation rates are never very high (Fig. 4f). The high occurrence of *Tuberculodinium vancampoae* in sapropel S3 sediments has been observed before (Zonneveld and Susek, 2007). Its high occurrence in an open-water setting could indicate the vicinity of the core site to an inshore lagoonal environment (Zonneveld et al., 2013). *T. vancampoae* becomes less dominant 1.5 kyrs after the onset of S3, when freshwater input and stratification continue to increase, favouring relative increases *of L. machaerophorum* and *Straurastrum*. This succession is consistent with a late maximum in insolation forcing (and relative monsoonal strength) during S3 (Fig. 6j).

In short, both sapropels clearly show enhanced inflow of Nile-derived water before and during sapropel deposition. Moreover, our proxies suggest that the influence of the Nile was stronger during S3 compared to S1. Some of this signal might relate to the lower sea level at the time of sapropel S3 (Figure 6k; Grant et al., 2016), resulting potentially in a Nile outflow closer to the core location. However, the $\delta^{18}O_{residuals}$ from the LC21 core (Grant et al., 2016) taken near Crete shows average values of −0.57‰ and −0.66‰ for S1 and S3, respectively. This is consistent with a higher North-African run-off during S3 relative to S1 also for that core location. Sea surface temperature (SST) increase may be amplified during sapropel formation, because of the amplified radiative gain of fresh water lenses (Emeis et al., 2003; Rodriguez-Sanz et al., 2017). Even though SST effects on $\delta^{18}O_{residuals}$ are considered to be low (Grant et al., 2016), the impact of SST on $\delta^{18}O_{ruber}$ may thus be underestimated. Data from Ocean Drilling Program (ODP) Site 967 indicate SSTs in a similar range (~17-21 °C) and at most ~1 °C higher during S1 compared to S3. This would relate to ~0.23‰ (Bemis et al., 1998) heavier values for SST-

corrected $\delta^{18}O_{residuals}$ during S1 compared to S3, suggesting an even higher difference in North-African river discharge during sapropels S1 and S3. As such, including or excluding this SST effect, we conclude that Nile discharge was stronger during S3 relative to S1, in line with the somewhat higher Northern Hemisphere summer insolation that occurred during S3 deposition and related enhanced monsoon intensity (Emeis et al., 2003) (Fig. 6j).

4.2. Vegetation variability in the Nile catchment

Besides transport and preservation changes, sedimentary pollen assemblages are recording changes in the vegetation of the Nile catchment and can therefore be applied to reconstruct larger (terrestrial) environmental changes, i.e. hydrological patterns (Hennekam et al., 2015a). Within both sapropels S1 and S3 pollen preservation is excellent. Changes in the terrestrial environment over time are best represented by the percent abundances with bisaccates types, typically overrepresented in marine records, excluded from the pollen sum. Previous studies from the same region and time period found assemblages similar to ours (e.g. Rossignol-Strick et al., 1982; Rossignol-Strick and Paterne, 1999; Cheddadi and Rossignol-Strick, 1995a; Langgut et al., 2011; Langgut, 2017). Sapropel S1, deposited during the well-known African Humid Period (AHP) (Box et al., 2011), has a clear two-phase development with a relatively moist first half, indicated by maxima in *Q. robur* and *Rumex*. Vegetation changes resemble those from core PS009PC offshore Israel (van Helmond et al., 2015) implying consistency in the main Nile outflow. The vegetation development across sapropel deposition shows broadly similar patterns between S1 and S3. Simultaneous increases during sapropel onset in *Artemisia*, Chenopodiaceae, *Quercus* and *Rumex,* at the expense of *Ephedra,* Cyperaceae and Poaceae, signal contrasting changes. *Quercus* and *Rumex* increases and *Ephedra* decline indicate a more humid climate in and around the Nile delta in the Eastern Mediterranean, corresponding well with the higher rainfall during sapropel deposition (e.g. Rossignol-Strick et al., 1982; Langgut et al., 2011; Langgut, 2017). In apparent contrast, the increased *Artemisia* and Chenopodiaceae typically signal dry conditions (Langgut et al., 2011). However, these same taxa occur in desert and semi-desert vegetation. Expansion of the semi-desert relative to sparse desert environments, indicated by the *Ephedra* decline, likely caused the increased *Artemisia* and Chenopodiaceae during onset of both sapropels S1 and S3. *Artemisia* and Chenopodiaceae are also abundant in coastal vegetation of salt marshes and we suggest their high abundances are additionally diagnostic of expanding coastal vegetation and coastal flooding (Fernández-Illescas et al., 2010; Langgut et al., 2011).

The relative decrease of Cyperaceae just before sapropel formation and the low percentage during its formation is unusual (Fig. 5g) as Cyperaceae usually has enhanced levels during periods of increased humidity and correspondingly have high percentages within sapropels (Desprat et al., 2013). However, Cyperaceae occur in a wide range of mainly humid ecological conditions, including freshwater coastal wetlands. As the Cyperaceae pollen are rather fragile, this cannot be related to preservation (Li et al., 2005). We speculate that the change from Cyperaceae to *Artemisia* and Chenopodiaceae does not indicate dry conditions, but reflects the change from a fresh-water to salt-water marsh environment due to sea level rise at sapropel onset, followed by a Nile delta progradation due to higher run off. Comparison of near-shore S1 records has previously indicated an eastward shift of the main Nile tributary reflected by a shift in Cyperaceae (Hennekam et al., 2015a). More seasonal rainfall distribution during sapropel periods could result in the creation of distinct wet and dry seasons, which could contribute to this signal as well. The comparison of

absolute and relative trilete spore abundances in both S1 and S3, previously used as an indicator of upland erosion during dry conditions (e.g. Langgut, 2017), shows that high trilete percentages in these records are mainly a result of decreased other pollen input and preservation prior and after sapropel deposition. Therefore, the relative amount of trilete spores in our record does not provide reliable information on the upland catchment dynamics.

The overall higher *Artemisia* and lower proportion of deciduous trees in S3 relative to S1 (but comparable amounts of *Ephedra*), point to an increased contribution of semi-arid vegetation at the expense of Mediterranean woodland. The vegetation differences between the sapropels are indicative of mean drier conditions or greater seasonal contrast during S3. This is in apparent contrast with the higher pollen influx and stronger stratification signals during S3, but would be in line with a more seasonal distribution of rainfall resulting from enhanced monsoon activity. These data confirm recent findings from low-resolution S1 and S3 records from the Levantine Basin (Langgut, 2017), which indicate that our observations are regionally consistent.

Multiproxy terrestrial hydroclimate records (pollen, oxygen isotopes, aquatic fauna and sediment properties) in the eastern Mediterranean indicate wetter interglacial conditions in the Northern Levant, with a superimposed wet interval during S3, and southward displacement of westerly rain belts during glacials (Gasse et al., 2015). Long transient model simulations, forced by insolation, greenhouse gas concentrations and North Hemisphere ice sheet expansion, indicate approximately equal levels of North African summer runoff to the Mediterranean basin for S1 and S3 (Ziegler et al., 2010). We hypothesize that the increased semi-arid vegetation during S3 relative to S1, combined with the regionally available model and proxy records, point to a more seasonal distribution of humidity during S3.

4.3. Marine productivity

Ba/Al and C_{org} clearly indicate enhanced productivity during both sapropels (Fig. 6d,f). Moreover, C_{org} also shows an increase from background values prior to S3 (at ~88 kyr BP), while for S1 C_{org} values are also higher prior to sapropel deposition when compared with post-sapropel values (Fig. 6d). This suggests an increased productivity before sapropel deposition. During the sapropels, the Ba/Al profiles point towards a similar export productivity for S1 and S3 in our core area (Fig. 6f), and C_{org} concentrations were also similar between sapropel S3 and, at least, S1a (Fig. 6d). The somewhat higher Ba compared to C_{org} during S1b may be related to diagenetic effects on Ba, as some Ba can be re-mobilized if strong sulphate reduction causes undersaturation of barite (Van Os et al., 1991; Mercone et al., 2001; Henkel et al., 2012), which could favour even stronger Ba build-up during less reducing conditions (as during S1b). C_{org} concentrations primarily reflect the initial organic matter fluxes once anoxic conditions are established (Reed et al., 2011). The observed C_{org} concentrations, supported by comparable changes in H/A ratio (Fig. 6g), thus largely confirm the similar magnitude of marine productivity inferred from Ba/Al during sapropels S1a and S3.

The dinocyst accumulation rates (Fig. 6e) and H/A ratio (Fig. 6g) suggest increased marine productivity already before the onset of sapropel S3, in line with C_{org}. In contrast, high productivity seems to develop only at the onset of sapropel S1. However, the sample resolution and the relatively short interval studied before S1 onset (to ~10.5 kyr BP) renders conclusions about productivity difficult at this site. Evidence for enhanced productivity ~1 kyr before S1 deposition with high accumulation rates of *Spiniferites* spp. has been observed in other cores in this region previously (e.g. Kholeif and Mudie, 2009; van Helmond et al., 2015). In the first part of S1,

until ~8.5 kyr, accumulation rates of oxygen resistant (and total) dinocyst species and H/A ratio increase, which would exclude an overprint of preservation in the productivity signal (Zonneveld et al., 2001; Versteegh et al., 2010). In sapropel S3, the first signs of an increase in productivity are observed in high *Spiniferites* spp. accumulation rates at ~88 kyr BP, ~2–2.5 kyr before the sapropel. However, at the onset of sapropel S3 the accumulation rate of the oxygen-resistant dinocyst species diminishes, while that of total dinocysts and H/A ratio increase, which could suggest a more important overprint of preservation (Fig. 6e,g) on the productivity signal.

Dinocyst-derived productivity seems to be very variable and slightly higher in the upper part of S3, from ~83.5 kyrs onwards. The role of productivity in sapropel formation has long been debated, but is thought to be an important contributor to the high organic carbon levels within the sapropel (e.g. Rohling, 1994; Gallego-Torres et al., 2011). Our data show a general increase in marine productivity prior to both sapropels (~2 and ~1 kyr for S3 and S1, respectively), which can, at least partially, be attributed to nutrients transported by the Nile River at this core location.

4.4. Sediment anoxia, preservation, and water column redox-clines

The profiles of U/Al, Mo/Al, S, and C_{org}/P_{tot} show high values in both sapropels, indicating bottom water anoxia during sapropels S1 and S3 (Fig. 3d–g). The consistently high values for all proxies indicative of anoxic conditions during both sapropels also suggest that preservation was high during both sapropels, which is further supported by the well-preserved dinocysts and pollen. Moreover, the low values for Mn support the low oxygen conditions during both sapropels and also demonstrate that post-depositional diagenesis ('burn-down') did not occur. The Mn peak, with

simultaneous minor troughs in C_{org}, Ba/Al, Mo/Al and C_{org}/P_{tot}, at ~8 kyr BP is evidence for an interruption in sapropel S1 formation, with sustained higher deep water ventilation rates and somewhat lower productivity. The event may be linked to the 8.2 kyr BP cooling recorded in Greenland ice cores, as simultaneous winter cooling has been observed in the areas of Mediterranean deep-water formation (e.g. Casford et al., 2003; Rohling and Pälike, 2005).

Sapropel S3 shows somewhat higher values of Mo/Al, S, and C_{org}/P_{tot} compared to S1, suggesting that seafloor conditions were likely somewhat more reducing during sapropel S3 (Fig. 3d–f). The higher sedimentary S concentrations prior to sapropel S3 formation are most likely related to diagenetic pyritisation, which often occurs below sapropels following downward sulphide diffusion (see Passier et al., 1996). Similarly, the very high S concentrations at the base of S1 are likely the (diagenetic) result of downward sulphide diffusion meeting upward-diffusing dissolved Fe^{2+}, as also observed by Mercone et al. (2001) for S1. Nonetheless, the absolute values of S concentrations in both sapropels can be used to define the strength of past oxygen limitation. The S values of 1–2 wt. % during S1 and S3, respectively, suggest anoxic bottom waters during deposition of both sapropels (Mercone et al., 2001), and more reducing conditions during S3 compared to S1 (Fig. 6i). In addition to S, the absolute Mo concentrations (i.e. ~20 ppm during S1 and ~80 ppm during S3) suggest that bottom waters were intermittently euxinic during S1 and (semi)permanently euxinic during deposition of S3 (Scott and Lyons, 2012) (Fig. 6h).

The covariation of Mo–U can be used to provide additional information on redox intensity and the operation of metal-(oxyhydr) oxides particulate shuttles, which can be used, in turn, to indicate redoxclines in the water column (e.g. Algeo and Tribovillard, 2009; Scholz et al., 2013). The higher enrichment of Mo:U (Fig. 7a),
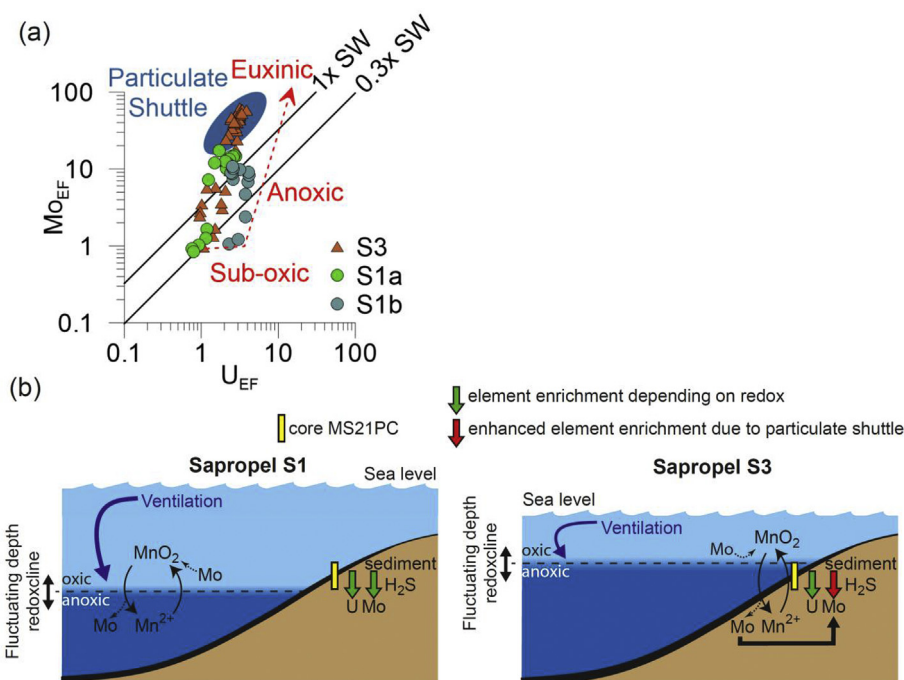
Fig. 7. (a) Enrichment factors (EF's) of Mo versus U. EF's were calculated by dividing Mo/Al and U/Al by their respective ratios in the post-Archean average shale (Taylor and McLennan, 1985; Algeo and Tribovillard, 2009). Data of sapropels S3 (brown triangles), S1a (light green circles), and S1b (dark green circles) are indicated. Solid black lines indicate sea water (SW) Mo/U ratio, and 0.3x fraction thereof. The area where "particulate shuttling" occurs in the modern-day Cariaco Basin is indicated with a blue oval area, while the pathway where sub-oxic, anoxic, and euxinic conditions occur are indicated with red, following Algeo and Tribovillard (2009). (b) Schematic model for water column processes (shown for Mn, but similar to Fe) and redox conditions during sapropels S1 (left) and S3 (right), inspired by Algeo and Tribovillard (2009), and based on data of *a*. The sea-level difference between both sapropels is indicated and exaggerated for clarity. (For interpretation of the references to colour in this figure legend, the reader is referred to the Web version of this article.)

relative to the sea water ratio (up to ~3-4x higher) suggests that particulate shuttling may have accelerated Mo enrichment, particularly during S3 (Algeo and Tribovillard, 2009). Mo has more affinity for adsorption to metal-(oxyhydr)oxides compared to U, and is therefore readily "shuttled" from the water column to the sediment by Mn- and Fe-(oxyhydr)oxide particles precipitated at the Mn- and Fe-redoxclines in the water column (i.e. particulate shuttling; Algeo and Tribovillard, 2009; Scholz et al., 2013). A prerequisite for this shuttle mechanism is the existence of an oxic-anoxic boundary in the water column. Moreover, frequent (i.e. decadal) renewal of bottom waters is necessary, because the Mn- and Fe particles would otherwise be reductively dissolved, releasing adsorbed Mo, before reaching the seafloor (Algeo and Tribovillard, 2009; Scholz et al., 2013).

These results suggest a highly fluctuating oxic-anoxic boundary within the water-column above 1022 m, the depth of MS21PC, during the entire interval between onset and termination of sapropel S3 (illustrated in Fig. 7b). During S1 we do not find evidence for such particulate shuttle mechanism at our core depth. This is consistent with observations based on a nearby core (880 m; Matthews et al., 2017), a basin-wide inferred redox-cline at ~1800m (De Lange et al., 2008), and deduced oxygen-free conditions during at least part of S1 at 1155 m for a site east of our core MS21PC (Bayon et al., 2013). Therefore, we conclude that anoxic conditions were not only enhanced, but also water-column ventilation was shallower during deposition of S3 relative to S1.

5. Synthesis and concluding remarks

Our geochemical and palynological data show that Nile discharge was higher during S3 than during S1. In contrast, the pollen assemblages and accumulation rates indicate increased semi-arid vegetation and reduced Mediterranean woodland cover during S3 relative to S1, which suggests that the increased Nile discharge can possibly be explained by a more seasonal distribution of humidity and runoff, while mean conditions were somewhat drier in S3 relative to S1. While this hypothesis needs further explicit testing, more seasonal rainfall distribution could explain the observed more pronounced stratification signal during S3. Lower global sea level during sapropel S3 compared to S1 could also be causing the amplified signal of the monsoon strengthening. Longer deep-water residence times in a more restricted Mediterranean basin (due to lower sea level) enhances the effect of basin-wide excess evaporation and causes higher initial salinities in the water column (e.g. Thunell et al., 1987; Rohling et al., 2014). The enhanced restriction during deposition of S3 likely resulted in a more pronounced density difference between freshwater (Nile discharge) and Mediterranean Sea water, causing enhanced stratification of the water column, thus reduced overturning circulation and ultimately stronger and shallower upper water depth for bottom water anoxia.

The magnitude of sedimentary and bottom-water anoxia during Eastern Mediterranean sapropels has often been related to North African monsoon strength, as the enhanced river discharge increased the buoyancy of surface waters and promoted stratification (e.g. Rossignol-Strick, 1985; Rohling, 1994; Rohling et al., 2015; Grant et al., 2016). The stronger effect of the monsoon observed in S3 compared to S1 can, similarly, be associated to higher water stratification during S3. Moreover, the existence of a particulate shuttle points towards a shallower ventilation during sapropel S3 compared to S1, which is probably also due to the higher run off from the Nile River.

The geochemical and palynological proxies point to high marine productivity during S1 (particularly the first phase) and S3. Additionally, dinocyst assemblages indicate that marine productivity increased prior to the onset of S3, likely associated with an increase in nutrient input from the Nile River. Higher export productivity and freshwater input likely resulted in increased organic matter production and acted as preconditioning factors even before the preservation overprint due to organic matter degradation became determinant for the deposition of the sapropel layer.

In conclusion, we show that the differences in orbitally-forced monsoon strength and related Nile River runoff had a significant effect on the water column processes and sea-floor redox conditions in the Eastern Mediterranean Sea during deposition of sapropels S1 and S3. This effect is amplified in S3 compared to S1, possibly aided by the lower sea level and thus greater restriction of the Mediterranean-Atlantic exchange during S3.

Acknowledgements

Appendix A. Supplementary data

Supplementary data related to this article can be found at https://doi.org/10.1016/j.quascirev.2018.08.026.

References

Algeo, T.J., Ingall, E., 2007. Sedimentary C org: P ratios, paleocean ventilation, and Phanerozoic atmospheric pO 2. Palaeogeogr. Palaeoclimatol. Palaeoecol. 256, 130—155.

Algeo, T.J., Tribovillard, N., 2009. Environmental analysis of paleoceanographic systems based on molybdenum—uranium covariation. Chem. Geol. 268 (3), 211—225.

Bar-Matthews, M., Ayalon, A., Gilmour, M., Matthews, A., Hawkesworth, C.J., 2003. Sea-land oxygen isotopic relationships from planktonic foraminifera and speleothems in the Eastern Mediterranean region and their implication for paleorainfall during interglacial intervals. Geochem. Cosmochim. Acta 67, 3181—3199.

Bayon, G., Dupré, S., Ponzevera, E., Etoubleau, J., Chéron, S., Pierre, C., Mascle, J., Boetius, A., De Lange, G.J., 2013. Formation of carbonate chimneys in the Mediterranean Sea linked to deep-water oxygen depletion. Nat. Geosci. 6 (9), 755.

Bemis, B.E., Spero, H.J., Bijma, J., Lea, D.W., 1998. Reevaluation of the oxygen isotopic composition of planktonic foraminifera: experimental results and revised paleotemperature equations. Paleoceanography 13.2, 150—160.

Beug, H.J., 2004. Leitfaden der Pollenbestimmung für Mitteleuropa und angrenzende Gebiete. Verlag Dr. Friedrich Pfeil.

Bernhardt, C.E., Horton, B.P., Stanley, J.-D., 2012. Nile Delta vegetation response to Holocene climate variability. Geology 40, 615—618.

Bishop, J.K.B., 1988. The barite-opal-organic carbon association in oceanic particulate matter. Nature 332, 341—343.

Blaauw, M., Christen, J.A., 2011. Flexible paleoclimate age-depth models using an autoregressive gamma process. Bayesian Analysis 6, 457—474.

Boaretto, E., Mienis, H.K., Sivan, D., 2010. Reservoir age based on pre-bomb shells from the intertidal zone along the coast of Israel. Nucl. Instrum. Meth. B 268, 966—968.

Box, M.R., Krom, M.D., Cliff, R.A., Bar-Matthews, M., Almogi-Labin, A., Ayalon, A., Paterne, M., 2011. Response of the Nile and its catchment to millennial-scale climatic change since the LGM from Sr isotopes and major elements of East Mediterranean sediments. Quat. Sci. Rev. 30, 431—442.

Casford, J.S.L., Rohling, E.J., Abu-Zied, R.H., Fontanier, C., Jorissen, F.J., Leng, M.J., Schmiedl, G., Thomson, J., 2003. A dynamic concept for eastern Mediterranean circulation and oxygenation during sapropel formation. Palaeogeogr. Palaeoclimatol. Palaeoecol. 190, 103—119.

Cheddadi, R., Rossignol-Strick, M., 1995a. Eastern Mediterranean Quaternary paleoclimates from pollen and isotope records of marine cores in the Nile cone area. Paleoceanography 10 (2), 291—300.

Cheddadi, R., Rossignol-Strick, M., 1995b. Improved preservation of organic matter and pollen in eastern Mediterranean sapropels. Paleoceanography 10, 301–309.

Cramp, A., O'Sullivan, G., 1999. Neogene sapropels in the Mediterranean: a review. Mar. Geol. 153, 11–28.

Dai, L., Weng, C., Lu, J., Mao, L., 2014. Pollen quantitative distribution in marine and fluvial surface sediments from the northern South China Sea: new insights into pollen transportation and deposition mechanisms. Quat. Int. 325, 136–149.

Danesh, D.C., McCarthy, F.M., Volik, O., Drljepan, M., 2013. Non-pollen paly-nomorphs as indicators of water quality in Lake Simcoe, Ontario, Canada. Palynology 37 (2), 231–245.

Desprat, S., Combourieu-Nebout, N., Essallami, L., Sicre, M.A., Dormoy, I., Peyron, O., Siani, G., Roumazeilles, V.B., Turon, J.L., 2013. Deglacial and Holocene vegetation and climatic changes in the southern Central Mediterranean from a direct land-sea correlation. Clim. Past 9 (2), 767.

De Lange, G.J., Thomson, J., Reitz, A., Slomp, C.P., Speranza Principato, M., Erba, E., Corselli, C., 2008. Synchronous basin-wide formation and redox-controlled preservation of a Mediterranean sapropel. Nat. Geosci. 1, 606–610.

De Rijk, S., Hayes, A., Rohling, E.J., 1999. Eastern Mediterranean sapropel S1 inter-ruption: an expression of the onset of climatic deterioration around 7 ka BP. Mar. Geol. 153, 337–343.

De Vernal, A., Marret, F., 2007. Chapter nine organic-walled dinoflagellate cysts: tracers of sea-surface conditions. Dev. Mar. Geol. 1, 371–408.

Dymond, J., Suess, E., Lyle, M., 1992. Barium in deep-sea sediment: a geochemical proxy for paleoproductivity. Paleoceanography 7 (2), 163–181.

Emeis, K.C., Schulz, H., Struck, U., Rossignol-Strick, M., Erlenkeuser, H., Howell, M.W., Kroon, D., Mackensen, A., Ishizuka, S., Oba, T., Sakamoto, T., 2003. Eastern Mediterranean surface water temperatures and δ18O composition during deposition of sapropels in the late Quaternary. Paleoceanography 18 (1), 1005.

Facorellis, Y., Maniatis, Y., Kromer, B., 1998. Apparent 14C ages of marine Mollusk shells from a Greek Island: calculation of the marine reservoir effect in the Aegean sea. Radiocarbon 40, 963–971.

Fensome, R.A., Williams, G.L., 2004. The Lentin and Williams Index of Fossil di-noflagellates, 2004 edition. In: American Association of Stratigraphic Palynol-ogists Contribution Series, vol. 42, p. 909.

Fernández-Illescas, F., Nieva, F.J.J., Silva, I., Tormo, R., Muñoz, A.F., 2010. Pollen production of Chenopodiaceae species at habitat and landscape scale in Med-iterranean salt marshes: an ecological and phenological study. Rev. Palaeobot. Palynol. 161 (3), 127–136.

Fontugne, M.R., Arnold, M., Labeyrie, L., Paterne, M., Calvert, S.E., Duplessy, J.C., 1994. Paleoenvironment, sapropel chronology and Nile River discharge during the last 20,000 years as indicated by deep-sea sediment records in the eastern Mediterranean. In: Bar-Yosef, O., Kra, R.S. (Eds.), Late Quaternary Chronology and Paleoclimates of the Eastern Mediterranean. Radiocarbon, Tucson, pp. 75–88.

Gallego-Torres, D., Martínez-Ruiz, F., Meyers, P.A., Paytan, A., Jiménez-Espejo, F.J., Ortega-Huertas, M., 2011. Productivity Patterns and N-fixation Associated with Pliocene-holocene Sapropels: Paleoceanographic and Paleoecological Significance.

Gasse, F., Vidal, L., Van Campo, E., Demory, F., Develle, A.L., Tachikawa, K., Elias, A., Bard, E., Garcia, M., Sonzogni, C., Thouveny, N., 2015. Hydroclimatic changes in northern Levant over the past 400,000 years. Quat. Sci. Rev. 111, 1–8.

Grant, K.M., Rohling, E.J., Bar-Matthews, M., Ayalon, A., Medina-Elizalde, M., Ramsey, C.B., Satow, C., Roberts, A.P., 2012. Rapid coupling between ice volume and polar temperature over the past 150,000 years. Nature 491, 744–747.

Grant, K.M., Grimm, R., Mikolajewicz, U., Marino, G., Ziegler, M., Rohling, E.J., 2016. The timing of Mediterranean sapropel deposition relative to insolation, sea-level and African monsoon changes. Quat. Sci. Rev. 140, 125–141.

Gray, D.D., Zonneveld, K.A., Versteegh, G.J., 2017. Species-specific sensitivity of dinoflagellate cysts to aerobic degradation: a five-year natural exposure experiment. Rev. Palaeobot. Palynol. 247, 175–187.

Grelaud, M., Marino, G., Ziveri, P., Rohling, E.J., 2012. Abrupt shoaling of the nutri-cline in response to massive freshwater flooding at the onset of the last inter-glacial sapropel event. Paleoceanography 27. PA3208.

Grimm, R., Maier-Reimer, E., Mikolajewicz, U., Schmiedl, G., Müller-Navarra, K., Adloff, F., Grant, K.M., Ziegler, M., Lourens, L.J., Emeis, K.C., 2015. Late glacial initiation of Holocene eastern Mediterranean sapropel formation. Nat. Com-mun. 6, 7099.

Head, M.J., 1993. Dinoflagellates, Sporomorphs, and Other Palynomorphs from the Upper Pliocene St. Erth Beds of Cornwall, Southwestern England. Memoir (The Paleontological Society), pp. 1–62.

Helz, G.R., Miller, C.V., Charnock, J.M., Mosselmans, J.F.W., Pattrick, R.A.D., Garner, C.D., Vaughan, D.J., 1996. Mechanism of molybdenum removal from the sea and its concentration in black shales: EXAFS evidence. Geochem. Cosmo-chim. Acta 60, 3631–3642.

Henkel, S., Mogollón, J.M., Nöthen, K., Franke, C., Bogus, K., Robin, E., Bahr, A., Blumenberg, M., Pape, T., Seifert, R., März, C., de Lange, G.J., Kasten, S., 2012. Diagenetic barium cycling in Black Sea sediments — a case study for anoxic marine environments. Geochem. Cosmochim. Acta 88, 88–105.

Hennekam, R., Jilbert, T., Schnetger, B., Lange, G.J., 2014. Solar forcing of Nile discharge and sapropel S1 formation in the early to middle Holocene eastern Mediterranean. Paleoceanography 29 (5), 343–356.

Hennekam, R., Donders, T.H., Zwiep, K., de Lange, G.J., 2015a. Integral view of Ho-locene precipitation and vegetation changes in the Nile catchment area as inferred from its delta sediments. Quat. Sci. Rev. 130, 189–199.

Hennekam, R., Jilbert, T., Mason, P.R.D., De Lange, G.J., Reichart, G.-J., 2015b. High-

resolution line-scan analysis of resin-embedded sediments using laser ablation-inductively coupled plasma-mass spectrometry (LA-ICP-MS). Chem. Geol. 403, 42–51.

Heusser, L., 1983. Pollen distribution in the bottom sediments of the western North Atlantic Ocean. Mar. Micropaleontol. 8 (1), 77–88.

Hilgen, F.J., 1991. Extension of the astronomically calibrated (polarity) time scale to the Miocene/Pliocene boundary. Earth Planet Sci. Lett. 107 (2), 349–368.

Kholeif, S.E., Mudie, P.J., 2009. Palynological records of climate and oceanic condi-tions in the late Pleistocene and Holocene of the Nile Cone, southeastern Mediterranean, Egypt. Palynology 33, 1–24.

Kotthoff, U., Pross, J., Müller, U.C., Peyron, O., Schmiedl, G., Schulz, H., Bordon, A., 2008. Climate dynamics in the borderlands of the Aegean Sea during formation of sapropel S1 deduced from a marine pollen record. Quat. Sci. Rev. 27 (7), 832–845.

Kraal, P., Slomp, C.P., De Lange, G.J., 2010. Sedimentary organic carbon to phos-phorus ratios as a redox proxy in Quaternary records from the Mediterranean. Chem. Geol. 277, 167–177.

Krom, M.D., Stanley, J.D., Cliff, R.A., Woodward, J.C., 2002. Nile River sediment fluctuations over the past 7000 yr and their key role in sapropel development. Geology 30, 71–74.

Langgut, D., Almogi-Labin, A., Bar-Matthews, M., Weinstein-Evron, M., 2011. Vege-tation and climate changes in the South Eastern Mediterranean during the Last Glacial-Interglacial cycle (86 ka): new marine pollen record. Quat. Sci. Rev. 30 (27), 3960–3972.

Langgut, D., 2017. Late quaternary nile flows as recorded in the Levantine Basin: the palynological evidence. Quat. Int. 1–12.

Laskar, J., Robutel, P., Joutel, F., Gastineau, M., Correia, A.C.M., Levrard, B., 2004. A long-term numerical solution for the insolation quantities of the Earth. Astron. Astrophys. 428, 261–285.

Li, Y.-C., Xu, Q.-H., Yang, X.-L., Chen, H., Lu, X.-M., 2005. Pollen-vegetation rela-tionship and pollen preservation on the northeastern qinghai-Tibetan plateau. Grana 44, 160–171.

Matthews, A., Azrieli-Tal, I., Benkovitz, A., Bar-Matthews, M., Vance, D., Poulton, S.W., Teutsch, N., Almogi-Labin, A., Archer, C., 2017. Anoxic develop-ment of sapropel S1 in the Nile Fan inferred from redox sensitive proxies, Fe speciation, Fe and Mo isotopes. Chem. Geol. 475, 24–39.

Matthiessen, J., Kunz-Pirrung, M., Mudie, P.J., 2000. Freshwater chlorophycean algae in recent marine sediments of the Beaufort, Laptev and Kara Seas (Arctic Ocean) as indicators of river runoff. Int. J. Earth Sci. 89 (3), 470–485.

McCarthy, F.M.G., Gostlin, K.E., Mudie, P.J., Hopkins, J.A., 2003. Terrestrial and ma-rine palynomorphs as sea-level proxies: an example from Quaternary sedi-ments on the New Jersey margin, U.S.A. In: Olson, H.C., Leckie, R.M. (Eds.), Micropaleontologic Proxies for Sea-level Change and Stratigraphic Disconti-nuities, pp. 119–129. SEPM Special Publication No. 75.

Mercone, D., Thomson, J., Abu-Zied, R.H., Croudace, I.W., Rohling, E.J., 2001. High-resolution geochemical and micropalaeontological profiling of the most recent eastern Mediterranean sapropel. Mar. Geol. 177, 25–44.

Mudie, P.J., 1982. Pollen distribution in recent marine sediments, eastern Canada. Can. J. Earth Sci. 19, 729–747.

Moss, P.T., Kershaw, A.P., Grindrod, J., 2005. Pollen transport and deposition in riverine and marine environments within the humid tropics of northeastern Australia. Rev. Palaeobot. Palynol. 134, 55–69.

Nijenhuis, I.A., Schenau, S.J., Van der Weijden, C.H., Hilgen, F.J., Lourens, L.J., Zachariasse, W.J., 1996. On the origin of upper Miocene sapropelites: a case study from the Faneromeni section, Crete (Greece). Paleoceanography 11 (5), 633–645.

Passier, H.F., Middelburg, J.J., Van Os, B.J.H., De Lange, G.J., 1996. Diagenetic pyriti-sation under eastern Mediterranean sapropels caused by downward sulphide diffusion. Geochem. Cosmochim. Acta 60, 751–763.

Passier, H.F., Middelburg, J.J., de Lange, G.J., Böttcher, M.E., 1999. Modes of sapropel formation in the eastern Mediterranean: some constraints based on pyrite properties. Mar. Geol. 153, 199–219.

Reed, D.C., Slomp, C.P., de Lange, G.J., 2011. A quantitative reconstruction of organic matter and nutrient diagenesis in Mediterranean Sea sediments over the Ho-locene. Geochem. Cosmochim. Acta 75, 5540–5558.

Reille, M., 1992. Pollen et spores d'Europe et d'Afrique du Nord. U.R.A. C.N.R.S., Marseille.

Reimer, P.J., McCormac, F.G., 2002. Marine radiocarbon reservoir corrections for the Mediterranean and Aegean Seas. Radiocarbon 44, 159–166.

Rochon, A., Vernal, A.D., Turon, J.L., Matthießen, J., Head, M.J., 1999. Distribution of recent dinoflagellate cysts in surface sediments from the North Atlantic Ocean and adjacent seas in relation to sea-surface parameters. Am. Assoc. Stratigr. Palynol. Contrib. Ser. 35, 1–146.

Rodríguez-Sanz, L., Bernasconi, S.M., Marino, G., Heslop, D., Mueller, I.A., Fernandez, A., Grant, K.M., Rohling, E.J., 2017. Penultimate deglacial warming across the Mediterranean Sea revealed by clumped isotopes in foraminifera. Sci. Rep. 7, 16572.

Rohling, E.J., Gieskes, W.W., 1989. Late Quaternary changes in Mediterranean in-termediate water density and formation rate. Paleoceanography 4, 531–545.

Rohling, E.J., 1994. Review and new aspects concerning the formation of eastern Mediterranean sapropels. Mar. Geol. 122, 1–28.

Rohling, E.J., Bigg, G.R., 1998. Paleosalinity and δ18O: A critical assessment. J. Geophys. Res. Oceans 103, 1307–1318.

Rohling, E.J., 1999. Environmental control on Mediterranean salinity and delta O-18. Paleoceanography 14, 706–715.

Rohling, E.J., De Rijk, S., 1999. Holocene Climate Optimum and Last Glacial Maximum in the Mediterranean: the marine oxygen isotope record. Mar. Geol. 153, 57—75.

Rohling, E.J., Cane, T.R., Cooke, S., Sprovieri, M., Bouloubassi, I., Emeis, K.C., Schiebel, R., Kroon, D., Jorissen, F.J., Lorre, A., Kemp, A.E.S., 2002. African monsoon variability during the previous interglacial maximum. Earth Planet Sci. Lett. 202, 61—75.

Rohling, E.J., Sprovieri, M., Cane, T., Casford, J.S.L., Cooke, S., Bouloubassi, I., Emeis, K.C., Schiebel, R., Rogerson, M., Hayes, A., Jorissen, F.J., Kroon, D., 2004. Reconstructing past planktic foraminiferal habitats using stable isotope data: a case history for Mediterranean sapropel S5. Mar. Micropaleontol. 50, 89—123.

Rohling, E.J., Pälike, H., 2005. Centennial-scale climate cooling with a sudden cold event around 8,200 years ago. Nature 434 (7036), 975—979.

Rohling, E.J., Foster, G.L., Grant, K.M., Marino, G., Roberts, A.P., Tamisiea, M.E., Williams, F., 2014. Sea-level and deep-sea-temperature variability over the past 5.3 million years. Nature 508 (7497), 477—482.

Rohling, E.J., Marino, G., Grant, K.M., 2015. Mediterranean climate and oceanography, and the periodic development of anoxic events (sapropels). Earth Sci. Rev. 143, 62—97.

Rohling, E.J., Hibbert, F.D., Williams, F.H., Grant, K.M., Marino, G., Foster, G.L., Hennekam, R., De Lange, G.J., Roberts, A.P., Yu, J., Webster, J.M., Yokoyama, Y., 2017. Differences between the last two glacial maxima and implications for ice-sheet, δ^{18}O, and sea-level reconstructions. Quat. Sci. Rev. 176, 1—28.

Rossignol-Strick, M., Nesteroff, W., Olive, P., Vergnaud-Grazzini, C., 1982. After the deluge: Mediterranean stagnation and sapropel formation. SMR (Somatosens. Mot. Res.) 1006, 34.

Rossignol-Strick, M., 1985. Mediterranean Quaternary sapropels, an immediate response of the African monsoon to variation of insolation. Palaeogeogr. Palaeoclimatol. Palaeoecol. 49, 237—263.

Rossignol-Strick, M., Paterne, M., 1999. A synthetic pollen record of the eastern Mediterranean sapropels of the last 1 Ma: implications for the time-scale and formation of sapropels. Mar. Geol. 153, 221—237.

Rossignol-Strick, M., 1999. The Holocene climatic optimum and pollen records of sapropel 1 in the eastern Mediterranean, 9000—6000 BP. Quat. Sci. Rev. 18, 515—530.

Sangiorgi, F., Capotondi, L., Combourieu Nebout, N., Vigliotti, L., Brinkhuis, H., Giunta, S., Lotter, A.F., Morigi, C., Negri, A., Reichart, G.J., 2003. Holocene seasonal sea-surface temperature variations in the southern Adriatic Sea inferred from a multiproxy approach. J. Quat. Sci. 18, 723—732.

Sangiorgi, F., Donders, T.H., 2004. Reconstructing 150 years of eutrophication in the north-western Adriatic Sea (Italy) using dinoflagellate cysts, pollen and spores. Estuar. Coast Shelf Sci. 60, 69—79.

Scholz, F., McManus, J., Sommer, S., 2013. The manganese and iron shuttle in a modern euxinic basin and implications for molybdenum cycling at euxinic ocean margins. Chem. Geol. 355, 56—68.

Scott, C., Lyons, T.W., 2012. Contrasting molybdenum cycling and isotopic properties in euxinic versus non-euxinic sediments and sedimentary rocks: refining the paleoproxies. Chem. Geol. 324—325, 19—27.

Slomp, C.P., Thomson, J., de Lange, G.J., 2002. Enhanced regeneration of phosphorus during formation of the most recent eastern Mediterranean sapropel (S1). Geochem. Cosmochim. Acta 66, 1171—1184.

Taylor, S.R., McLennan, S.M., 1985. The Continental Crust: Its Composition and Evolution. Blackwell Science, Oxford.

Thomson, J., Mercone, D., de Lange, G.J., van Santvoort, P.J.M., 1999. Review of recent advances in the interpretation of Eastern Mediterranean sapropel S1 from geochemical evidence. Mar. Geol. 153, 77—89.

Thunell, R.C., Williams, D.F., Howell, M., 1987. Atlantic-Mediterranean water exchange during the Late Neocene. Paleoceanography 2 (6), 661—678.

Tribovillard, N., Algeo, T.J., Lyons, T., Riboulleau, A., 2006. Trace metals as paleoredox and paleoproductivity proxies: An update. Chem. Geol. 232, 12—32.

Tribovillard, N., Algeo, T.J., Baudin, F., Riboulleau, A., 2012. Analysis of marine environmental conditions based on molybdenum—uranium covariation—Applications to Mesozoic paleoceanography. Chem. Geol. 324, 46—58.

van Helmond, N.A.G.M., Hennekam, R., Donders, T.H., Bunnik, F.P., de Lange, G.J., Brinkhuis, H., Sangiorgi, F., 2015. Marine productivity leads organic matter preservation in sapropel S1: palynological evidence from a core east of the Nile River outflow. Quat. Sci. Rev. 108, 130—138.

Van Os, B.J.H., Middelburg, J.J., De Lange, G.J., 1991. Possible diagenetic mobilization of barium in sapropelic sediment from the eastern Mediterranean. Mar. Geol. 100, 125—136.

Van Santvoort, P.J.M., De Lange, G.J., Thomson, J., Cussen, H., Wilson, T.R.S., Krom, M.D., Ströhle, K., 1996. Active post-depositional oxidation of the most recent sapropel (S1) in sediments of the eastern Mediterranean Sea. Geochem. Cosmochim. Acta 60 (21), 4007—4024.

Venkatarathnam, K., Ryan, W.B., 1971. Dispersal patterns of clay minerals in the sediments of the eastern Mediterranean Sea. Mar. Geol. 11 (4), 261—282.

Versteegh, G.J., Zonneveld, K.A., de Lange, G.J., 2010. Selective aerobic and anaerobic degradation of lipids and palynomorphs in the Eastern Mediterranean since the onset of sapropel S1 deposition. Mar. Geol. 278 (1), 177—192.

Waelbroeck, C., Labeyrie, L., Michel, E., Duplessy, J.C., McManus, J.F., Lambeck, K., Balbon, E., Labracherie, M., 2002. Sea-level and deep water temperature changes derived from benthic foraminifera isotopic records. Quat. Sci. Rev. 21, 295—305.

Weldeab, S., Siebel, W., Wehausen, R., Emeis, K.C., Schmiedl, G., Hemleben, C., 2003. Late Pleistocene sedimentation in the Western Mediterranean Sea: implications for productivity changes and climatic conditions in the catchment areas. Palaeogeogr. Palaeoclimatol. Palaeoecol. 190, 121—137.

Wood, G.D., Gabriel, A.M., Lawson, J.C., 1996. Palynological techniques — processing and microscopy. In: Jansonius, J., McGregor, D.C. (Eds.), Palynology: Principles and Applications, vol. 1. American Association of Stratigraphic Palynologists Foundation, Dallas, TX, pp. 29—50.

Ziegler, M., Tuenter, E., Lourens, L.J., 2010. The precession phase of the boreal summer monsoon as viewed from the eastern Mediterranean (ODP Site 968). Quat. Sci. Rev. 29, 1481—1490.

Zonneveld, K.A.F., Versteegh, G.J.M., De Lange, G.J., 2001. Palaeoproductivity and post-depositional aerobic organic matter decay reflected by dinoflagellate cyst assemblages of the Eastern Mediterranean S1 sapropel. Mar. Geol. 172, 181—195.

Zonneveld, K.A.F., Susek, E., 2007. Effects of temperature, light and salinity on cyst production and morphology of Tuberculodinium vancampoae (the resting cyst of Pyrophacus steinii). Rev. Palaeobot. Palynol. 145 (1), 77—88.

Zonneveld, K.A.F., Chen, L., Möbius, J., Mahmoud, M.S., 2009. Environmental significance of dinoflagellate cysts from the proximal part of the Po-river discharge plume (off southern Italy, Eastern Mediterranean). J. Sea Res. 62, 189—213.

Zonneveld, K.A.F., Marret, F., Versteegh, G.J., Bogus, K., Bonnet, S., Bouimetarhan, I., Crouch, E., de Vernal, A., Elshanawany, R., Edwards, L., Esper, O., 2013. Atlas of modern dinoflagellate cyst distribution based on 2405 data points. Rev. Palaeobot. Palynol. 191, 1—197.